

pubs.acs.org/biochemistry Article

# Descriptive Analysis of Transient-State Observations for Thioredoxin/Glutathione Reductase (Sec597Cys) from *Schistosoma mansoni*

Madison M. Smith, Tyler B. Alt, David L. Williams, and Graham R. Moran\*



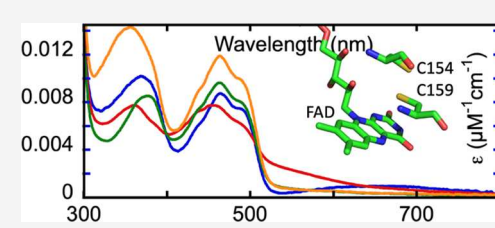
Cite This: Biochemistry 2023, 62, 1497-1508



**ACCESS** 

Metrics & More

ABSTRACT: Thioredoxin/glutathione reductase from *Schistosoma mansoni* (SmTGR) catalyzes the reduction of both oxidized thioredoxin and glutathione with electrons from reduced nicotinamide adenine dinucleotide phosphate (NADPH). SmTGR is a drug target for the treatment of Schistosomiasis, an infection caused by *Schistosoma* platyhelminths residing in the blood vessels of the host. *Schistosoma* spp. are reliant on TGR enzymes as they lack catalase and so use reduced thioredoxin and glutathione to regenerate peroxiredoxins consumed in the detoxification of reactive oxygen species. SmTGR is a flavin adenine dinucleotide



Article Recommendations

(FAD)-dependent enzyme, and we have used the flavin as a spectrophotometric reporter to observe the movement of electrons within the enzyme. The data show that NADPH fractionally reduces the active site flavin with an observed rate constant estimated in this study to be  $\sim 3000~\rm s^{-1}$ . The flavin then reoxidizes by passing electrons at a similar rate to the proximal Cys159–Cys154 disulfide pair. The dissociation of NADP<sup>+</sup> occurs with a rate of  $\sim 180~\rm s^{-1}$ , which induces the deprotonation of Cys159, and this coincides with the accumulation of an intense FAD-thiolate charge transfer band. It is proposed that the electrons then pass to the Cys596–Cys597 disulfide pair of the associated subunit in the dimer with a net rate constant of  $\sim 2~\rm s^{-1}$ . (Note: Cys597 is Sec597 in wild-type (WT) SmTGR.) From this position, the electrons can be passed to oxidized thioredoxin or further into the protein to reduce the Cys28–Cys31 disulfide pair of the originating subunit of the dimer. From the Cys28–Cys31 center, electrons can then pass to oxidized glutathione that has a binding site directly adjacent.

# INTRODUCTION

Schistosomiasis is a parasitic infection caused by the platyhelminth *Schistosoma mansoni* and is common in tropical and subtropical countries. The mortality rate from this disease has dropped significantly in the last 30 years, due to the efficacy of treatment with praziquantel. However, evidence for praziquantel resistance is emerging, exposing the need for the development of new therapeutic agents. Several factors have slowed the development of new drugs for schistosomiasis including storage/transport limitations, low financial incentives, and that Schistosoma are formidable and resilient parasites. According to the World Health Organization, the development of new treatments for Schistosomiasis is a current priority.

Schistosomes undergo a complex life cycle in the blood-stream of the infected individual. Throughout this life cycle, the schistosome is subjected to oxidative stress via reactive oxygen species generated as a byproduct of their own aerobic respiration and as a part of the host immune response. To detoxify these reactive oxygen species, *Schistosoma* have high levels of superoxide dismutase but oddly lack catalase. These organisms instead rely on peroxiredoxins to ameliorate the oxidative effects of  $H_2O_2$  and require reduced forms of both glutathione (GSH) and thioredoxin ( $Trx_{\rm red}$ ) to reinstate the

reduced forms of the peroxiredoxins.<sup>7–9</sup> To maintain constant intracellular levels of GSH and Trx<sub>red</sub>, the reduced forms must be regenerated via reductase activities. In most eukaryotes, this requires two enzymes, glutathione reductase (GR) and thioredoxin reductase (TrxR). However, *Schistosoma* utilize a single enzyme, thioredoxin/glutathione reductase (SmTGR), which has both GR and TrxR activities, and as such regenerates both GSH and Trx<sub>red</sub>. This difference in the maintenance of redox homeostasis has resulted in SmTGR being identified via RNA interference as critical for the parasite's survival and is therefore a drug target for the treatment of schistosomiasis.

As the name suggests, TGR enzymes deliver reducing equivalents from nicotinamide adenine dinucleotide phosphate (NADPH) to both oxidized glutathione (GSSG) and thioredoxin ( $Trx_{ox}$ ); sustaining the cytosolic supply of reductants. The structure of TGR enzymes is known and is

Received: January 30, 2023 Revised: March 31, 2023 Published: April 18, 2023





similar to both GR and TrxR from higher organisms and all three have a fold similar to lipoamide dehydrogenase. However, TGR has an appended N-terminal domain that imparts GSSG reductase activity. TGR, GR, and TrxR function as homodimers with each subunit noncovalently binding a flavin adenine dinucleotide (FAD) cofactor and possessing functional cysteine pairs that form redox relays for electron transmission by alternating between disulfide and dithiol states (Figure 1). GR has one catalytic disulfide directly adjacent to

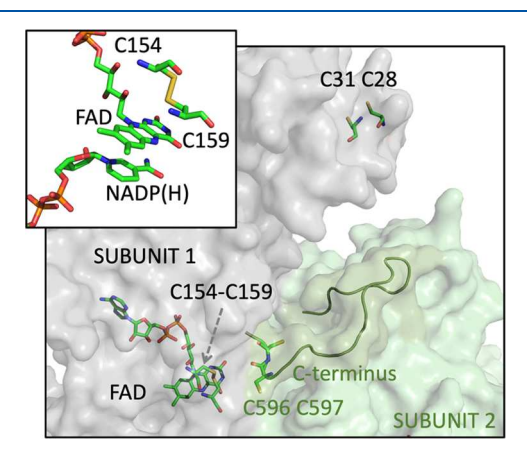


**Figure 1.** Structure of SmTGR rendered from PDB ID 2X8C. The two subunits of the TGR homodimer are shown in gray and green. The image highlights the relative positions of the redox centers. It is proposed that the C-terminal 596–597 cysteine pair of the adjacent subunit is dynamic and can receive electrons from the 154–159 cysteine pair and either reduce thioredoxin or extend to reduce the 28–31 disulfide that is adjacent to a binding site for GSSG. The inset depicts the arrangement of NADP and FAD relative to the 154–159 disulfide and was generated from PDB ID 2X99.

the flavin isoalloxazine. <sup>12</sup> TrxR has an additional dynamic C-terminal sulfide—selenide bonded pair (Cys—Sec) that is thought to shuttle electrons to  $\text{Trx}_{ox}$  that binds proximally. <sup>13</sup> TGR has a third catalytic disulfide that resides in the appended N-terminal domain that binds reduces GSSG. <sup>11,14</sup> Though no direct evidence supports the electron relay mechanism of the TGR disulfides, it is thought that the C-terminal cysteine pair serves to reduce both the disulfide of  $\text{Trx}_{ox}$  and the N-terminal domain disulfide for reduction of GSSG.

TGR enzymes have been studied using X-ray crystallography, redox titrations, and steady-state analysis.  $^{11,14-17}$  We report the first comprehensive transient-state analysis of a TGR enzyme. Changes in the FAD cofactor absorption spectrum indicate rapid fractional reduction by NADPH and rapid reoxidation to ultimately form a quasi-equilibrium distribution of electrons among all redox active entities within the enzyme. And while proposed in the absence of direct evidence, this process appears kinetically gated by the movement of the disordered C-terminus that carries the C596-C597 disulfide and delivers electrons either to Trx or to the C28-C31 disulfide that reduces GSSG. This sharing of electrons permits the flavin to continue to report evidence of electron distribution changes long after reduction of the proximal C154-C159 disulfide. As a result, a staged reoxidation of the flavin is observed as electrons distribute within the protein to presumably reduce more distant disulfides. While the data obtained were complicated by apparent interdimer electron transfer, these and other observations have permitted the tentative assignment of the steps of the TGR catalytic cycle.

#### MATERIALS AND METHODS

Materials, Quantitation, and Reaction Conditions. Reduced nicotinamide adenine dinucleotide phosphate (NADPH) was purchased from RPI Research Products. Lysogeny broth (LB) agar tablets were obtained from Bio101, Inc. Competent BL21 (DE3) cells were obtained from New England BioLabs. Dipotassium hydrogen phosphate (KPi), ethylenediaminetetraacetic acid (EDTA), oxidized nicotinamide adenine dinucleotide phosphate (NADP+), the Miller formulation of lysogeny broth (LB) powder, and sodium dodecylsufate (SDS) were purchased from Fisher Scientific. Talon superflow resin was purchased from Cytvia. Kanamycin was purchased from Alfa Aesar. Flavin adenine dinucleotide (FAD) was from Acros. Saccharomyces cerevisiae hexokinase was from Alfa Aesar and Leuconostoc mesenteroides glucose-6phosphate dehydrogenase was purchased from MP Biomedicals. 1D-D-Glucose was from Cambridge Isotopes. Reduced nicotinamide adenine dinucleotide (NADH) was purchased from Amresco. Adenosine triphosphate (ATP) was from Millipore-Sigma.

Where possible, concentrations were determined spectro-photometrically using the following extinction coefficients: NADPH or NADH;  $\varepsilon_{340}=6220~\mathrm{M^{-1}~cm^{-1}}$ , NADP+;  $\varepsilon_{260}=17,800~\mathrm{M^{-1}~cm^{-1}}$ , thioredoxin (SmTrx);  $\varepsilon_{280}=9500~\mathrm{M^{-1}~cm^{-1}}$ , ATP; the extinction coefficient used to quantify SmTGR was based on the absorption of the FAD cofactor and measured to be  $\varepsilon_{463}=11,700~\mathrm{M^{-1}~cm^{-1}}$  (see below). The concentration of oxidized glutathione was defined by weight. All reactant concentrations indicated in this text are post-mixing. All experiments were performed in 50 mM KPi pH 7.4 at 20 °C.

Expression and Purification of SmTGR and SmTrx. Expression and purification of SmTGR, and SmTrx was achieved using adaptations of standard protocols. The genes for S. mansoni TGR Sec597Cys and Trx were synthesized and subcloned into the pET28a+ expression plasmid by Genscript using NdeI and XhoI restriction sites to give the plasmids pSmTGR and pSmTrx, respectively. This placed both genes in phase with the sequence coding for an N-terminal 6His-tag linked by a thrombin cleavage site. Both plasmids were transformed separately into competent BL21 (DE3) Escherichia coli cells. Cell stocks were prepared by transferring one colony to an LB growth culture with 25  $\mu$ g/mL kanamycin and grown with shaking at 220 rpm at 37 °C until the culture showed the first signs of turbidity. 1 mL cell stocks were prepared by mixing 400  $\mu$ L of 0.22  $\mu$ m filtered 50% glycerol with 600  $\mu$ L aliquots of the culture and stored at -80 °C.

To express from plasmids pSmTGR and pSmTrx, 100  $\mu$ L of the BL21 (DE3) cell stock was spread onto an LB agar plate with 25  $\mu$ g/mL kanamycin selection and incubated at 37 °C for 16 h. The resulting cell lawn was resuspended with sterile LB broth and used to inoculate 1 L of LB broth with the appropriate antibiotic as indicated above. Cells were grown at 37 °C with shaking (220 rpm) to an optical density at 600 nm of 0.8, equilibrated to 25 °C for 1 h, and induced by the addition of 100  $\mu$ M isopropyl- $\beta$ -thiogalactopyranoside. The culture was then incubated at this temperature with shaking for an additional 20 h.

Protein purification was undertaken at 4 °C. Cells were harvested by centrifugation at 3500g for 35 min and the cell pellet was resuspended in ~100 mL of 50 mM KPi and 100 mM NaCl, pH 7.4. After resuspension (50  $\mu$ M FAD was added

to the SmTGR cell slurry) the solution was kept on ice for  $\sim 10$ min to allow for equilibration prior to sonication. The suspension was lysed by sonication for 8 min using a Branson 450 sonifier set to 40 W. Cellular debris was separated by centrifugation at 10,000g for 1 h. The supernatant was loaded onto a Talon affinity column ( $10 \times 1.25 \text{ cm}^2$ ) preequilibrated with 50 mM KPi, 100 mM NaCl, and 10 mM imidazole, pH 7.4. Proteins were eluted using a 400 mL gradient from 10 to 300 mM imidazole in 50 mM KPi, 100 mM NaCl, pH 7.4 and collected in 5 mL fractions. Fractions within the gradient elution showing significant absorption at 280 nm were pooled (FAD (100–150  $\mu$ M) was added to the pooled SmTGR sample and the solution was kept on ice for  $\sim 10$  min to allow for equilibration). For the SmTGR sample denaturation of what is assumed to be apoenzyme in the sample was acheived by dividing the sample into 50 mL polypropylene screw cap tubes and placing in a 55 °C water bath for 5 min. This heat treatment was determined to have no impact on the total activity of the sample and was used routinely as a method to eliminate, what is assumed to be, unstable states of apoenzyme. The precipitated apoenzyme was separated via centrifugation at 10,000g for 15 min at 4 °C. Pure protein samples were concentrated and buffer-exchanged into 50 mM KPi, pH 7.4, using Amicon Ultra-15, 10 kDa nominal molecular weight cutoff centrifugal filters. The concentrated sample was quantified by absorption at 463 nm and assayed prior to being stored at −80 °C.

Dialysis was also utilized as a method of exchanging buffer and was found to preserve more total active enzyme than repeated centrifugal concentration. Prior to dialysis, the enzyme was heat-treated and the precipitate was removed as stated above. The sample was then transferred to a hydrated Slide-a-Lyzer cassette (Pierce) and placed into a volume of buffer equivalent to at least 200 times the sample volume. The buffer was stirred using a magnetic stir bar for at least 1.5 h at 4 °C, after which the buffer was discarded and replaced with fresh 50 mM KPi, pH 7.4, and stirred for ~16 h. The sample was removed from the cassette, heat-treated, and the precipitate removed as above. Complete removal of free FAD was verified using the ratio of absorbance at 280–460 nm. The turnover number was also verified to be the same irrespective of the buffer exchange method.

Determination of the Extinction Coefficient for FAD Bound to SmTGR. To quantify the SmTGR concentration most investigators have used the extinction coefficient of the FAD cofactor ( $\varepsilon_{450 \text{ nm}} = 11,300 \text{ M}^{-1} \text{ cm}^{-1}$ ). However, upon examination of the enzyme spectrum, there appears to be clear perturbation of the flavin spectrum when bound to the enzyme. To determine a more representative extinction coefficient for the quantification of SmTGR,  $\sim$ 10  $\mu$ M enzyme was added to a cuvette containing 100 mM NaPi and 1 mM EDTA, pH 7.3. This solution was heated to 55 °C and an absorption spectrum was collected. To the same cuvette, 1.1% SDS was added to denature the protein. The solution was maintained at 55 °C for ~10 min to allow for full denaturation, with repeated spectra collected every ~3 min until changes were no longer observed. The final spectrum collected was for unbound FAD and was corrected for dilution. The known extinction coefficient for free FAD was used to determine the extinction coefficient of FAD when bound to SmTGR.

**Steady-State Analysis of SmTGR.** Aerobic steady-state measurements were obtained separately for SmTrx and GSSG, both in the presence of saturating NADPH and varied

concentrations of the oxidant substrate. All aerobic assays were performed in 50 mM KPi, pH 7.4 with a final reaction volume of 1 mL. In a quartz cuvette, a solution containing 150 μM NADPH (final) and a defined concentration of oxidant was prepared. GSSG concentrations were varied from 0 to 320  $\mu$ M, and SmTrx concentrations were varied from 0 to 292  $\mu$ M. The reaction was initiated by the addition of 500 nM SmTGR. The rate of NADPH oxidation was monitored at 340 nm for approximately 2 min using a Shimadzu UV-2600 spectrophotometer. The slope was determined for the most linear portion, between 50 and 120 s. Anaerobic steady-state measurements were undertaken using a stopped-flow instrument. SmTGR (2  $\mu$ M) was prepared in a tonometer as described below. This was mixed with a solution containing 150  $\mu$ M NADPH and a defined concentration of oxidant substrate. For GSSG the NADPH, oxidant solution was prepared by sparging as described below. For SmTrx, double-mixing stopped flow was utilized. The oxidant substrate was drawn into the stopped-flow instrument and mixed with varied ratios of anaerobic buffer supplied from the fourth syringe, and the concentration was verified by collecting an absorption spectrum. The enzyme was then mixed with the SmTrx solution aged for 0.1 s and mixed with NADPH. The steadystate rate was defined between 20 and 60 s. The measured rates were divided by the SmTGR concentration and plotted against oxidant concentration and then fit to the Michaelis-Menten equation (eq 1), using KaleidaGraph software. In this equation, Av. TN is the average turnover number calculated by dividing the measured rate in units of concentration per unit time by the enzyme concentration.

Av. TN = 
$$\frac{TN[S]}{K_m + [S]}$$
 (1)

Transient-State Analysis of SmTGR under Anaerobic Conditions. Enzyme samples were made anaerobic in glass tonometers using a Schlenk line and alternating cycles of vacuum and pure argon according to published protocols. 18 The tonometer was then mounted onto a HiTech stoppedflow spectrophotometer (TgK Scientific). Solutions that included substrates and products were made anaerobic in buffer by sparging for 5 min with argon and mounting onto the stopped-flow spectrophotometer. It was observed that the addition of glucose and glucose oxidase destabilized SmTGR and so enzymatic dioxygen scrubbing was not employed. However, 1 mM glucose with 1 U/mL glucose oxidase, made anaerobic as described above, was introduced to the stoppedflow instrument to scrub the system of molecular oxygen and prior to experiments, this solution was displaced by anaerobic buffer prepared by sparging with argon.

The observed rate constants in SmTGR Sec597Cys reactions span 5 orders of magnitude. For this reason, stopped-flow data were commonly collected for two time-frames and spliced together at the limit of the shorter acquisition to form a single trace. This process is necessary to provide adequate temporal resolution to describe both rapid and slow events as the spacing of data points in the longer acquisitions is too large to adequately describe fast initial steps.

SmTGR Reductive Half-Reaction with Limiting NADPH. To characterize the reductive half-reaction of SmTGR, concentrations of NADPH ranging from 5 to 40  $\mu$ M were mixed with 50.2  $\mu$ M SmTGR under anaerobic conditions using a stopped-flow spectrophotometer. For each concentration of NADPH, the reaction was monitored at a

Biochemistry pubs.acs.org/biochemistry Article

single wavelength using photomultiplier detection. Two timeframes (0.0012-0.2 and 0.0012-500 s) were collected for each concentration at each wavelength. The two data sets corresponding to a specific concentration and wavelength were spliced together at 0.2 s to provide adequate resolution to describe rapid and relatively slow processes. The 460 and 540 nm traces were fit to a linear combination of three exponentials, eq 2, using KaleidaGraph software. In this equation, X is the wavelength of observation,  $A_n$  is the amplitude associated with phase n,  $k_{\rm obsn}$  is the observed rate constant for phase *n*, *t* is time in s, and *C* is the absorbance end point. The reaction between 40  $\mu M$  NADPH and 50.2  $\mu M$ SmTGR was also monitored using charge coupled device (CCD) detection to obtain time-resolved spectra. The CCD data were collected on two timeframes, 0.0016-2.53 s and 0.0016-500 s, and spliced together at 2.53 s to provide adequate time resolution. The resulting data set was deconvoluted using singular value decomposition and subsequently fit to an irreversible three-step model using KinTek Explorer software.

$$A_{Xnm} = \left(\sum_{n=1}^{x} \Delta A_n (e^{-k_{\text{obsn}}t})\right) + C$$
(2)

To assess the influence of interdimer redox processes, the dependence of the events observed during the reductive halfreaction on the concentration of SmTGR was evaluated. SmTGR (80  $\mu$ M initial) was prepared anaerobically as described above. Varied volumes of the enzyme solution were then drawn into the stopped-flow instrument and mixed in varied ratios with anaerobic buffer to yield a range of SmTGR concentrations. For each dilution, an absorption spectrum was collected in the instrument to measure the SmTGR concentration (9.9, 11.0, 18.5, 28.5  $\mu$ M). These solutions were then individually mixed with NADPH (10  $\mu$ M), and the reaction was observed at 460 and 540 nm under anaerobic conditions at 20  $^{\circ}$ C. The reactions were observed for two timeframes (0.0012-0.2 and 0.0012-(200-500) s) and the traces were spliced together at 0.2 s. The traces were fit to a linear combination of three exponential terms according to eq

NADP<sup>+</sup> Titration to SmTGR. NADP<sup>+</sup> is a product of the SmTGR reaction and likely would compete with NADPH for the enzyme's active site at high concentrations. To determine a relative binding constant for NADP+ and define how its presence influences the system,  $0-320 \mu M \text{ NADP}^+$  with 13  $\mu$ M NADPH was titrated to 13.5  $\mu$ M SmTGR using a stoppedflow spectrophotometer under anaerobic conditions. The reaction was monitored at 450 nm to observe flavin reduction and reoxidation, and at 540 nm to monitor the accumulation and decay of charge transfer species. For both wavelengths, two timeframes were collected (0.0012-0.2 and 0.0012-100 s) and spliced together at 0.2 s. All data were brought to the same starting point for improved discernment of the observed trends. Each trace was fit to three exponentials according to eq 2 using KaleidaGraph software. The fits were used analytically to measure amplitude changes and define an apparent  $K_d$  for NADP<sup>+</sup> binding by fitting to eq 3. In this equation,  $K_{\text{dapp}}$ represents the apparent dissociation constant for NADP+ in the presence of NADPH.

$$\Delta Abs_{540nm} = \frac{\Delta Abs_{max}[NADP^+]}{K_{dapp} + [NADP^+]}$$
(3)

Influence of Oxidant Substrates on the Oxidation State of the FAD Cofactor. The effect of GSSG on the reductive half-reaction was analyzed using anaerobic transient-state methods. Substrate solutions, containing 8.9  $\mu$ M NADPH and varied concentrations of GSSG (0–160  $\mu$ M), were mixed with 10.5  $\mu$ M SmTGR using a stopped-flow spectrophotometer. The reaction was monitored at 460 nm for two timeframes, 0.0012–0.2 and 0.0012–1000 s. The two data sets for each concentration were spliced together at 0.2 s.

The effect of SmTrx on the net oxidation state of the FAD was analyzed using anaerobic transient-state methods. Doublemixing stopped flow was used to minimize the impact of a slow background reaction of NADPH with SmTrx. A solution of 8.9 μM NADPH was prepared, made anaerobic as described above, and mounted onto the stopped-flow spectrophotometer. The same was done for SmTrx concentrations ranging from 0 to 116  $\mu$ M. A 10.5  $\mu$ M sample of SmTGR was also made anaerobic as described above and mounted onto the stopped-flow spectrophotometer. For each data set collected, the NADPH and SmTrx solutions were first mixed with an age time of 0.1 s, before being mixed with the enzyme solution. The reaction was monitored at 460 nm for two timeframes, 0.0012-0.2 and 0.0012-200 s. The two data sets for each concentration were spliced together at 0.2 s. The data was fit analytically to four exponentials (eq 2) using KaleidaGraph

Kinetic Isotope Effects (KIE) with [4S- $^2$ H] NADPH as a Substrate. [4S- $^2$ H] NADPH and NADPH were synthesized enzymatically using an equivalent protocol. 1D-D-Glucose and D-glucose were separately phosphorylated and oxidized using a combination of *S. cerevisiae* hexokinase (300 nM) and *L. mesenteroides* glucose-6-phosphate dehydrogenase (30 nM). The reaction mixture included 200  $\mu$ M NADP $^+$ , 1 mM 1D-D-glucose or D-glucose, 400  $\mu$ M adenosine 5'-triphosphate (ATP), and 10 mM magnesium sulfate. The reaction was allowed to come to equilibrium ( $\sim$ 1500 s) at which time ostensibly all NADP $^+$  was reduced and the enzymes were removed using 10 kDa cutoff centrifugal filters at 4 °C. The resulting filtrate was then diluted to target NADPH/D concentrations and used immediately in kinetic experiments.

The effect of [4S- $^2$ H] NADPH on the reductive half-reaction of SmTGR was observed by mixing with either NADPH or [4S- $^2$ H] NADPD ( $\sim$ 7.0 and  $\sim$ 12.0  $\mu$ M) under anaerobic conditions at 20  $^{\circ}$ C. The reactions were observed at 460 and 540 nm for two timeframes (0.0012–0.2 and 0.0012–200 s) and the traces were spliced together at 0.2 s. To assess rate constant changes, the traces were each fit to a linear combination of three exponential terms according to eq 2 using KaleidaGraph Software.

# ■ RESULTS AND DISCUSSION

The anthelmintic praziquantel is active against numerous parasitic worm infections. *S. mansoni* is sensitive to praziquantel and three doses in a single day is usually sufficient to clear the infection. In endemic areas, a single annual dose is commonly used to suppress and/or eliminate the infection in addition to reducing the number of eggs shed into the environment. However, as the sole treatment available for schistosomiasis, <sup>19</sup> the continued use of praziquantel is

# Scheme 1. Proposed Sequences of Catalysis in SmTGR

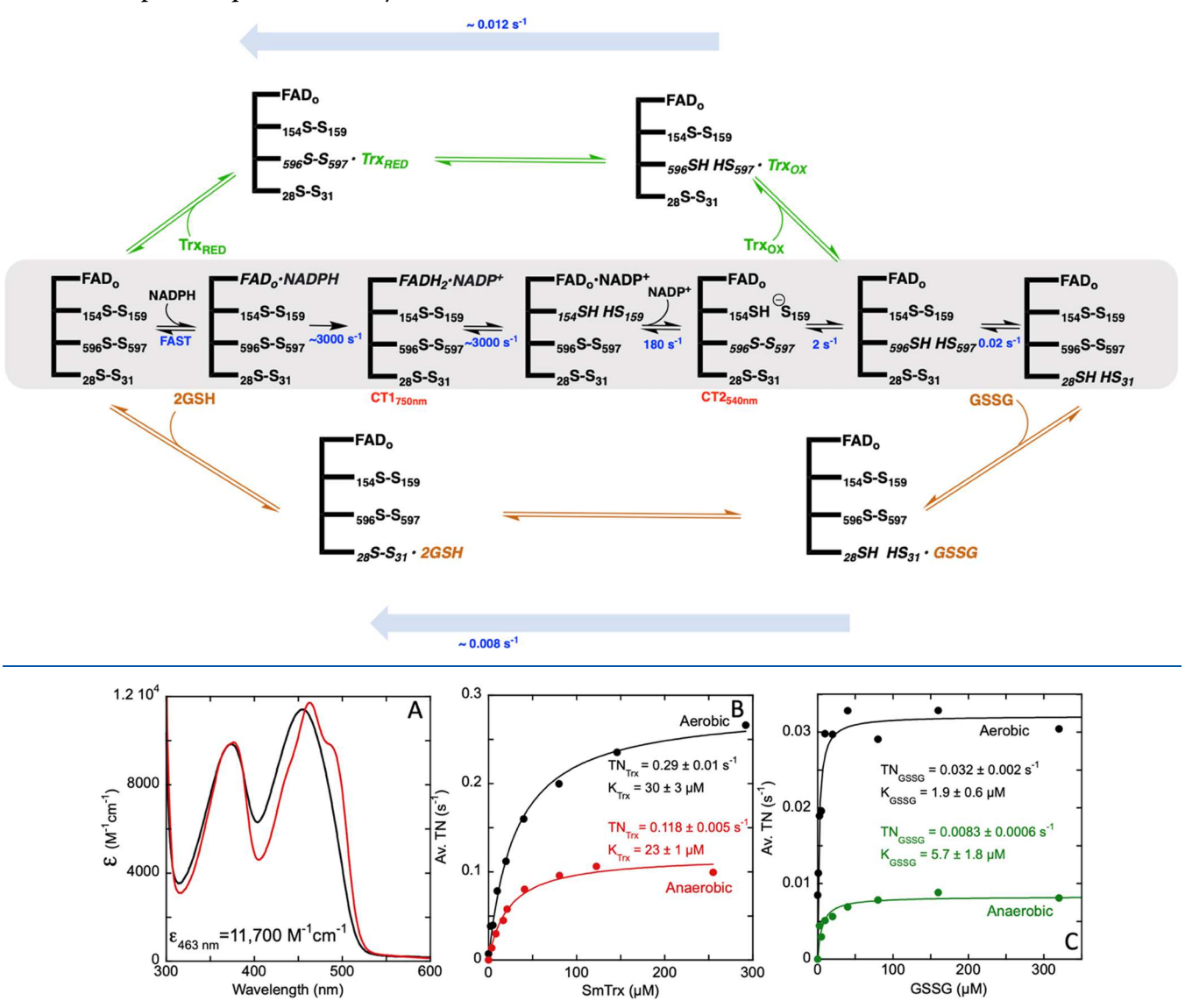


Figure 2. Spectrophotometric and steady-state analysis of SmTGR. (A) Extinction coefficient of FAD bound to SmTGR was determined by heating SmTGR ( $\sim$ 10  $\mu$ M) in 100 mM NaPi, 1 mM EDTA at pH 7.3 to 55 °C, and the absorption spectrum was recorded. SDS was then added to 1.1% (110  $\mu$ L), and the denaturation of TGR was allowed to proceed for 10 min at which time the spectrum was again recorded. The latter spectrum was corrected for dilution, and the extinction coefficient spectrum for SmTGR was derived based on the known extinction of unbound FAD (11,300 M<sup>-1</sup> cm<sup>-1</sup>). The spectra shown are SmTGR (red spectrum) vs free FAD (black spectrum). (B) Aerobic vs anaerobic steady-state analysis of SmTGR with SmTrx as the oxidant substrate. For each aerobic measurement, SmTGR (500 nM) in 50 mM KPi, pH 7.4 was combined with NADPH (150  $\mu$ M) and varied SmTrx. Anaerobic measurements were obtained by mixing SmTGR (0.9  $\mu$ M) in 50 mM KPi, pH 7.4 with NADPH (150  $\mu$ M) and varied SmTrx in a stopped-flow spectrophotometer. The reaction was observed for approximately 2 min, and the data from 20 to 60 s was used to define the rate at each oxidant concentration. (C) Aerobic vs anaerobic steady-state curves for GSSG. The anaerobic curve was obtained by mixing SmTGR (2  $\mu$ M) in 50 mM KPi, pH 7.4 with NADPH (150  $\mu$ M) and varied GSSG on a stopped-flow spectrophotometer. For both (B) and (C), Michaelis—Menten analyses in which the oxidant substrates were titrated observed 340 nm. These data provided rates of the decrease in absorption that occurred with the oxidation of NADPH. The average turnover was plotted against oxidant substrate concentration and fit to the Michaelis—Menten equation (eq 1). Each curve is derived from a single experiment and so includes no error analysis representative of reproducibility. The error indicated is from the goodness of fit for each curve.

vulnerable to the development of resistant *Schistosoma* and evidence for attenuated efficacy has been reported.<sup>4</sup> Given that nearly 200 million people have schistosomiasis and that 0.3 million die annually of the disease, the need for additional methods of treatment is plainly apparent.

TGR is an enzyme whose function is pivotal for the survival of parasitic platyhelminthes. The reason for this is that these organisms typically do not have catalase and so rely heavily on the activity of TGR to maintain an overall reducing environment within their cells and TGR has been validated as a drug target by RNAi inhibition. Despite its therapeutic importance no comprehensive transient-state kinetic studies have been undertaken and relatively little is known of its catalytic cycle or the mechanism(s) of susceptibility to candidate inhibitors. Here we present the first characterization of the reductive and oxidative events that occur in the two catalytic cycles of SmTGR. This study was facilitated by mutagenesis of the 597 selenocysteine codon to that of a

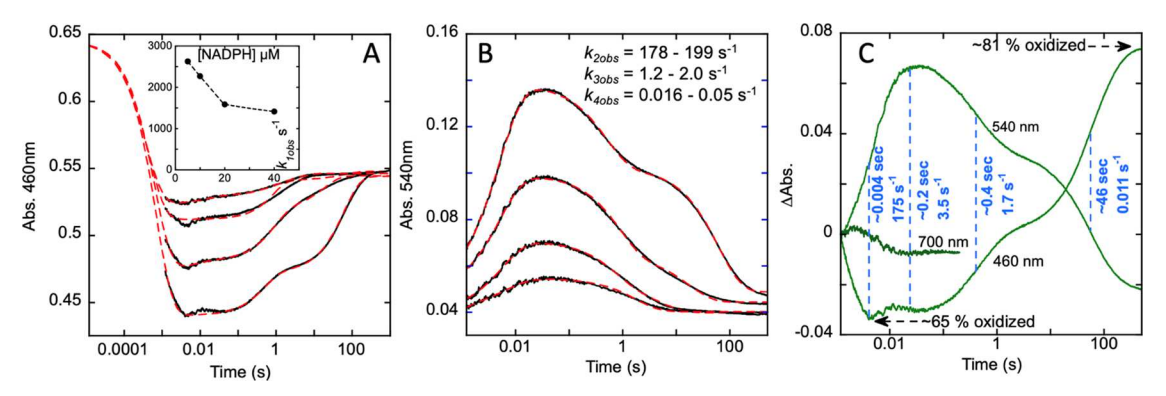


Figure 3. Reductive half-reaction of SmTGR. SmTGR (50.2  $\mu$ M) was mixed with NADPH (5, 10, 20, 40  $\mu$ M) under anaerobic conditions at 20 °C. The reaction was observed at 460 nm (A) and 540 nm (B) for 500 s and at 700 nm for 0.2 s. The 500 s traces were spliced together from 0.2 and 500 s logarithmic data sets to provide adequate temporal resolution for all phases. In (A), the starting absorbance is artificially defined as the value for the oxidized enzyme at 460 nm for 50.2  $\mu$ M SmTGR. The inset in (A) shows estimates of the rate for the first phase based on the fits shown (red dashed lines). (C) Overlay of the data obtained with 40  $\mu$ M NADPH at the three wavelengths. Dashed vertical lines indicate approximate half-lives for the phases observed facilitating visual correlation for individual processes for each wavelength. The rapid flavin reduction phase is not annotated in this manner as the first time point is beyond the half-life for this phase. The data for each wavelength were artificially brought to the same starting point solely to facilitate visual comparison. The extent oxidized was estimated based on the known time-zero absorption at 460 nm and the extinction coefficient change for the reduction of FAD. Each is indicated with a tilde as the latter is not known for SmTGR.

cysteine, which permits the use of conventional *E. coli* heterologous expression methods yielding substantially more purified TGR than is obtained from expression systems that include the added components required for selenocysteine incorporation. <sup>20,21</sup> In addition, the kinetic behavior of the Sec > Cys variant form of TGR has been shown to be only modestly different from that of the wild-type form. <sup>14,17</sup> Moreover, the function of Sec in proteins does not appear to alter the overall chemistry and is thought to be incorporated only to imbue resilience to oxidative inactivation for the residue. <sup>22–25</sup>

Here we take advantage of the absorption changes that occur for the flavin cofactor. For TGR the transitions of the flavin are augmented by FAD·thiolate and FADH $_2$ ·NADP $^+$  charge transfer absorption that provide added evidence for the sequence of catalytic events. Our results and tentative conclusions are summarized in Scheme 1.

Purification and Quantitation of SmTGR. SmTGR Sec597Cys was expressed in BL21 DE3 cells overnight at 25 °C. Purification yielded ~40 mg of purified enzyme per liter of culture. The yield of SmTGR activity was enhanced approximately 2-fold by adding FAD (50  $\mu$ M) during sonication and after chromatographic elution (125  $\mu$ M). Incubation of the enzyme sample at 55 °C for 5 min was used to denature and remove, what is assumed to be apo and/ or misfolded-SmTGR and did not diminish the total units of activity. Without heating to denature apo-SmTGR, the enzyme sample is prone to accumulate turbidity. Purified and heattreated TGR samples returned 280/460 nm absorbance ratios of  $\sim$ 7.5. SmTGR prepared in this manner can be stored at -80°C indefinitely without loss of activity upon thawing. Purified SmTGR was quantified using the measured extinction coefficient of  $\varepsilon_{463} = 11,700 \text{ M}^{-1} \text{ cm}^{-1}$  (Figure 2A). The spectrum observed for FAD bound to SmTGR has near-visible absorption maximum at 375 nm, ostensibly the same as free FAD, and a long-wavelength maximum at 463 nm with the long-wavelength transitions resolving to a pronounced shoulder at 480 nm. This spectrum is very similar to spectra reported for other TGR preparations and for GRs and TrxRs. 14,26-28

Steady-State Analysis. Anaerobic steady-state analysis while titrating the oxidant substrates, GSSG and SmTrx, indicates that the limiting rate of turnover is 10-fold slower for GSSG (0.0083 s<sup>-1</sup>) relative to SmTrx (0.12 s<sup>-1</sup>), but the  $K_{\rm m}$ value for GSSG is approximately 15-fold lower so that the  $k_{\text{cat}}$ /  $K_{\rm m}$  values for both substrates are similar at  $\sim 10^4~{\rm M}^{-1}~{\rm s}^{-1}$ (Figure 2B,C). The enzyme exhibits a clear preference for NADPH compared to NADH with  $k_{\rm cat}/K_{\rm m}$  values of 8.9 × 10<sup>3</sup>  $\pm$  659 and 69.3  $\pm$  13 M<sup>-1</sup> s<sup>-1</sup>, respectively (data not shown). Aerobic steady-state measurements indicate reactivity with dioxygen in that the apparent aerobic turnover numbers are ~3-fold and ~4-fold more for SmTrx and GSSG, respectively. The greater difference in rate between anaerobic and aerobic turnover for GSSG is consistent with the slower rate of reduction for this substrate providing more opportunity for electrons to return to the flavin by disulfide exchange redistribution and then presumably be lost to hydrogen peroxide production. These data also indicate limited veracity for turnover numbers from prior steady-state observations for TGR that were universally carried out under aerobic conditions. 14,17

Transient-State Analysis of the Reductive Half-Reaction. The reductive half-reaction of SmTGR was observed by mixing the enzyme with NADPH under anaerobic conditions. This reaction can be monitored at all wavelengths between 300 and 800 nm, though the most diagnostic changes occur at absorption maxima for NADPH, FAD, and at wavelengths ~540 and ~700 nm where charge transfer species can be observed independent of other chromophores. In Figure 3A,B, we show transient-state data for the reductive half-reaction at 460 and 540 nm that respectively report the net flavin oxidation state and charge transfer arising from FAD-thiolate proximity.

These data indicate five phases, each of which has a dependence on the NADPH concentration used. The first phase is rapid and is largely complete within the dead-time of the stopped-flow instrument (0.0012 s). This phase was assigned as fractional reduction of the FAD cofactor by hydride transfer from NADPH. Corroborative evidence is an absorption feature observed at 700 nm whose accumulation

is maximal at the dead-time, indicative of an FADH<sub>2</sub>-NADP<sup>+</sup> charge transfer species (Figure 3C). The amplitude of the flavin reduction phase at 460 nm is limited by an ensuing rapid increase in absorption that can be observed as a small increase immediately following flavin reduction. Fitting to four exponential terms according to eq 2 returned approximate rate constant values of 1000-2500 s<sup>-1</sup> for flavin reduction followed by a rate of 160-175 s<sup>-1</sup> that is provisionally assigned as deprotonation of the 159 thiol that occurs after rapid reoxidation of the FAD by reduction of the adjacent 154-159 disulfide. The reduction and reoxidation of the flavin have nearly equivalent extinction coefficient changes and what is observed is that both processes converge in terms of amplitude to arrive at a fractionally reduced state for the flavin immediately after partial Cys154-Cys159 disulfide reduction. This indicates that the end of the second phase corresponds to an equilibrium position where electrons are shared between the FAD, NADP, and the nearby 154-159 disulfide. Concomitant with the second phase is a large increase in absorption centered around 540 nm that is tentatively assigned here as deprotonation of now cysteine 159 (the most proximal cysteine to the flavin, Figure 1) to form a FAD-thiolate charge transfer absorption band that extends into the region of FAD absorption transitions and to longer wavelengths.1

While maximal accumulation of the 540 nm absorption feature corresponds to the maximal fractional state of FAD reduction, this state is only 35% reduced and so is consistent with arising from the proximity of the thiolate with the oxidized form of the flavin. That the apparent FADH<sub>2</sub>-NADP<sup>+</sup> charge transfer absorption at 700 nm decays completely with a rate constant of  $\sim 175~\rm s^{-1}$  indicates that NADP<sup>+</sup> is likely dissociating with this observed rate constant as the form of the enzyme accumulating with this event is the maximally reduced state for any given NADPH concentration. It is conceivable that egress of NADP<sup>+</sup> is required to provide electrostatic or conformational conditions conducive to Cys159 deprotonation (see below). These data that describe the initial steps of the SmTGR reductive half-reaction are notably similar to data reported by Huber and Brandt for glutathione reductase.  $^{29}$ 

Two additional phases are observed that result in nearcomplete reoxidation of the flavin for NADPH concentrations significantly less than that of the enzyme. These phases are most apparent at 460 and 540 nm in Figure 3 and occur with rate constant ranges of 1-2 and 0.02-0.05 s<sup>-1</sup>, both roughly 10-fold more rapid than the turnover numbers measured in steady-state for SmTrx and GSSG, respectively (Figure 2B,C). These two latter phases are tentatively assigned to the net flow of electrons away from the flavin with progressively further reach at higher NADPH concentrations. This would result in successive reduction, the 596-597 and then the 28-31 disulfides. As such, what is observed at 460 nm at any point in time is the net state of reduction of the FAD as a reporter for the quasi-equilibrium of states that occur with the distribution of electrons within the redox centers of SmTGR. Figure 3C illustrates the overlaid absorption changes observed at 460, 540, and 700 nm with approximate half-lives for the phases indicated and so permits visual correlation of the chemical sequence observed. For reasons described above, this figure does not include an estimate of the half-life for the first phase.

The stepped nature of the reoxidation of the flavin is most apparent at the highest limiting NADPH concentrations that are approximately equimolar with the enzyme. This indicates that intervening reduced states for disulfide centers accumulate

to increased extents when more electrons are provided to the system and therefore in a net sense, the electrons can penetrate further populating more distant disulfides. That each NADPH concentration does not yield a trace that has proportional amplitudes for FAD reoxidation in phases 4 and 5 suggests the system has added redox complexity outside the linear progression of 154–159 to 596–597 to 28–31 disulfides. Similar staged oxidation of the FADH<sub>2</sub> has been observed in GR from *Plasmodium* in the presence of GSSG. <sup>27,30</sup> Given that glutathione reductases have only one catalytic disulfide that is positionally equivalent and functionally similar to 154–159 in SmTGR, they must employ a different, and likely more direct, mechanism to reduce GSSG, indicating that observation stepped reoxidation alone does not permit definitive assignment of these events.

Available X-ray crystal structures reveal that the 596-597 cysteine pair is at the end of a 17 amino acid C-terminus without a defined secondary structure. This presumed flexible section of peptide is seemingly required to provide a means to pass electrons from 154 to 159 near the FAD to bound Trx and the 28-31 disulfide that is ~42 Å distant. However, this dynamic section of peptide likely also adds considerable complexity from intra- and interdimer redox activity. Most particularly at low NADPH concentrations with respect to the enzyme, the sample has a high fraction of enzyme that is fully oxidized and likely prone to adventitious interdimer redox chemistry. Qualitative evidence of this phenomenon is that for low NADPH concentrations, the flavin returns to near fully oxidized suggesting that a significant fraction of the electrons that were introduced ultimately reside on other enzyme subunits that did not encounter NADPH.

**Deconvolution of Time-Dependent Absorption Data Sets.** The large number of unique redox states for TGR and the sensitive spectrophotometric evidence from the FAD cofactor added to two charge transfer states for specific complexes provide an opportunity to further characterize the reductive half-reaction using spectral deconvolution protocols. To accomplish this SmTGR (50.2  $\mu$ M) was mixed with NADPH (40  $\mu$ M) under anaerobic conditions and the reaction was observed at all wavelengths between 300 and 800 nm using stopped-flow spectrophotometry with charged coupled device detection. A spliced data set was compiled from averaged data collected for two timeframes. This data set was fit to a linear irreversible three-step model and returned rate constants of 182, 2.1, and 0.017 s<sup>-1</sup>, largely consistent with the observed rate constants measured using single-wavelength, photomultiplier detection (Figure 3). As such the spectra returned from singular value decomposition do not represent pure discrete states of the enzyme's catalytic cycle and instead show the composite spectra for delineated stages in the progression of the reductive half-reaction (Figure 4).

These data did not include evidence for the  $t_{\rm zero}$  spectrum as the phase that consumes this state is too rapid to be captured even using an integration time that provides greatest time resolution (0.0016 s). For this reason, Figure 4 includes a reconstructed  $t_{\rm zero}$  spectrum compiled from the SmTGR spectrum added to the contribution of added NADPH (dashed spectrum). The first state observed is projected to have maximal accumulation at  $\sim$ 0.0002 s and is clearly composed of partially reduced flavin added to long-wavelength charge transfer absorption centered around 650 nm (blue spectrum). That this charge transfer transition does not overlap with the flavin spectrum allows for an accounting of

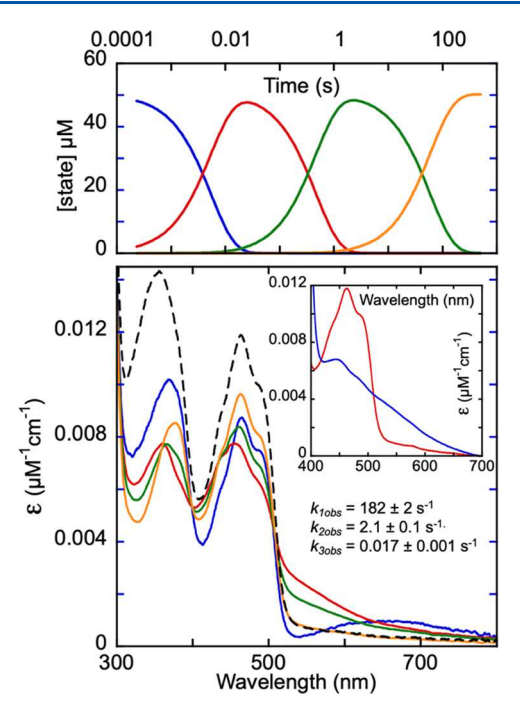


Figure 4. Spectral deconvolution of the reductive half-reaction of SmTGR. SmTGR (50.2  $\mu$ M) was mixed with NADPH (40  $\mu$ M) under anaerobic conditions at 20 °C. The reaction was observed using CCD data collection from 300 to 800 nm. Data were collected on two timeframes: 0.0016-2.53 s and 0.0016-500 s. Each data set was the average of two. The averaged data sets were spliced together at 2.53 s to provide optimal time resolution. The combined data set was deconvoluted using singular value decomposition and fit to a linear irreversible three-step model. This method thus does not account for equilibria between redox centers and reports spectra indicative of composite states defined by the phases observed. As such, the concentration profile derived from the fit (top) represents only the transitions between the states shown. Due to the rapid rate of reduction by NADPH, the rate of decay and the spectrum for time zero (black dashed spectrum) could not be obtained from this analysis. This spectrum was reconstructed from the spectrum for SmTGR added to the spectrum for 40  $\mu$ M NADPH and converted based on the SmTGR FAD extinction coefficient. The inset depicts the spectra of over-reduced SmTGR. SmTGR (6.4  $\mu M$ ) (initial spectrum shown in red) was combined with NADPH (640  $\mu$ M) and the system was left to come to equilibrium for 1800 s (final spectrum in blue).

reduced states at this stage of catalysis. This is not as straightforward for subsequent states as the absorption contribution of the flavin is overlapped with the ensuing broad FAD-thiolate charge transfer absorption such that the additive contributions of each chromophore cannot be known (Figure 4, inset). Assuming a change in extinction coefficient for flavin reduction of ~8500 M<sup>-1</sup> cm<sup>-1</sup> at 460 nm, the first spectrum captured has 35% flavin reduced which in this experiment equates to 17.6 µM. However, changes in absorption at 340 nm, which is commonly an isosbestic point for flavin oxidized and reduced spectra,  $^{31}$  show 32  $\mu M$ NADPH oxidation. This illustrates that the majority of the NADPH is consumed in reduction of the flavin but the flavin is rapidly reoxidizing by both reduction of the nearby 154-159 disulfide and reduction of NADP+ formed. That not all of the NADPH is oxidized at the end of the first phase suggests both that the FAD has an unusually low reduction potential and that electrons pass reversibly between the three redox active

species: NADPH, FAD, and the 154–159 disulfide. An unusually low reduction potential of –366 mV for the FAD of *E. coli* GR has also been reported.<sup>32</sup>

Interestingly, the above estimates of oxidized and reduced species permit the added conclusion that the  $\sim 180 \text{ s}^{-1}$  phase observed is not the rate constant of reduction of the 154-159 disulfide but instead reports the deprotonation of the 159 thiol. The basis for this conclusion is that the initial state revealed by deconvolution has no evidence of FAD-thiolate charge transfer absorption. In other words, in this experiment, FAD-thiolate charge transfer develops after 154-159 disulfide reduction with a rate constant of 180 s<sup>-1</sup>, which is likely also the rate of egress of NADP+ as the long-wavelength charge transfer species decays with the accumulation of the FAD-thiolate charge transfer transitions. This then allows the further conclusion that the rate constant for flavin reduction by NADPH and then reoxidation by reduction of the 154-159 disulfide are comparable such that only ~35% of the reduced flavin is observed to accumulate, moreover that maximal accumulation of the reduced state occurs at an extrapolated time of 0.0002 s indicates these rate constants are on the order of  $3000 \text{ s}^{-1}$ .

The 182 s<sup>-1</sup> phase forms the maximally accumulated state for the FAD-thiolate charge transfer which then decays at 2.1 s<sup>-1</sup> diminishing the thiolate charge transfer by 30%. This is tentatively assigned as a net migration of electrons to reduce the 596-597 disulfide. That electrons accumulate at this juncture in the relay of successive disulfides suggests a kinetic barrier to further distribution toward the 28-31 disulfide. It is reasonable to imagine that this barrier arises from the requirement for extensive reorganization of the C-terminus such that the 596-597 dithiol can come into contact with the 28-31 disulfide (or disulfides on other SmTGR subunits) (Figure 1). The ensuing event with a rate constant of  $0.017 \text{ s}^{-1}$ is not, as will be shown below, rate of migration of electrons toward the 28-31 disulfide. The extent of reoxidation of the flavin during this phase is dependent on the concentration of added NADPH and very little reoxidation is observed when NADPH concentrations are well above that of the enzyme (data not shown), which clearly demonstrates that more than two electrons can enter the enzyme via the flavin to potentially form two- to eight-electron reduced states. It can also be concluded that neither of these events is observed to occur with intrinsic rates for these steps as their combined effect returns the enzyme to a partially reduced state indicating that electrons are shared among the redox centers in the absence of recipient oxidant substrate(s) (see below).

Influence of NADP+ on the Reductive Half-Reaction. The data described above indicate loss of weak longwavelength charge transfer transitions concomitant with accumulation of intense short-wavelength charge transfer. As stated, this suggests that dissociation of NADP+ from stacked proximity with the re-face of the flavin isoalloxazine promotes deprotonation of Cys159 yielding the new charge transfer absorption. To evaluate the influence of NADP+, this product was titrated during observation of the SmTGR reductive halfreaction (Figure 5). The data obtained show that NADP<sup>+</sup> has no influence on the rate of flavin reduction, at least to the extent that this process can be observed. This suggests that the affinity for NADP+ is low and/or that the affinity for NADPH is relatively high. The data also show that repopulation of the NADP<sup>+</sup> site on the reduced enzyme suppresses FAD-thiolate charge transfer accumulation consistent with dissociation of

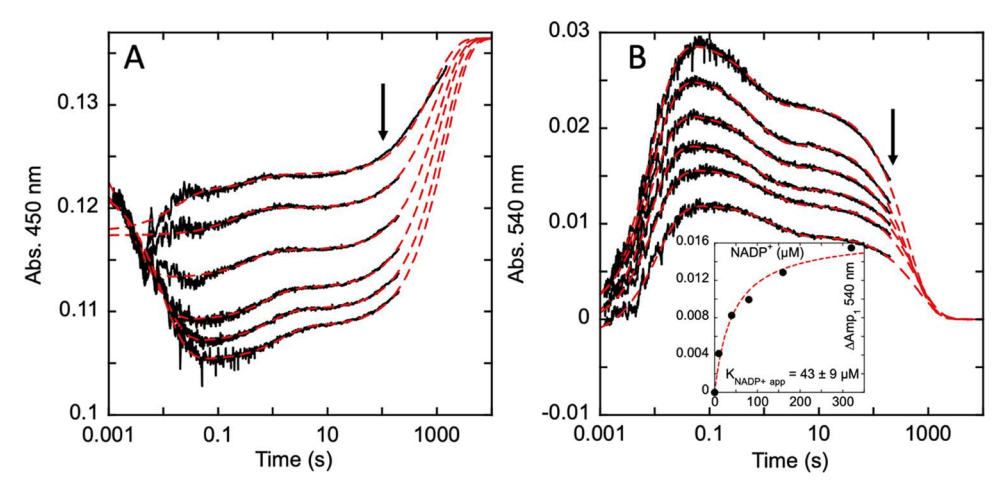


Figure 5. Influence of NADP<sup>+</sup> on the reductive half-reaction of SmTGR. SmTGR (13.5  $\mu$ M) was mixed with NADPH (13  $\mu$ M) and a range of NADP<sup>+</sup> concentrations (0, 10, 40, 80, 160, 320  $\mu$ M) under anaerobic conditions at 20 °C. The reaction was observed at 450 nm (A) and 540 nm (B) for two timeframes (0.0012–0.2 and 0.0012–100 s) and the 100 s traces shown were spliced together at 0.2 s to provide adequate time resolution for all phases. The traces were fit to a linear combination of three exponential terms. Arrows indicate increasing NADP<sup>+</sup> concentration. The inset shows the relationship of the amplitude of the first phase observed at 540 nm to the concentration of NADP<sup>+</sup>. This curve was fit to a single-site binding equation (eq 3) to determine an apparent  $K_d$  for NADP<sup>+</sup> binding.

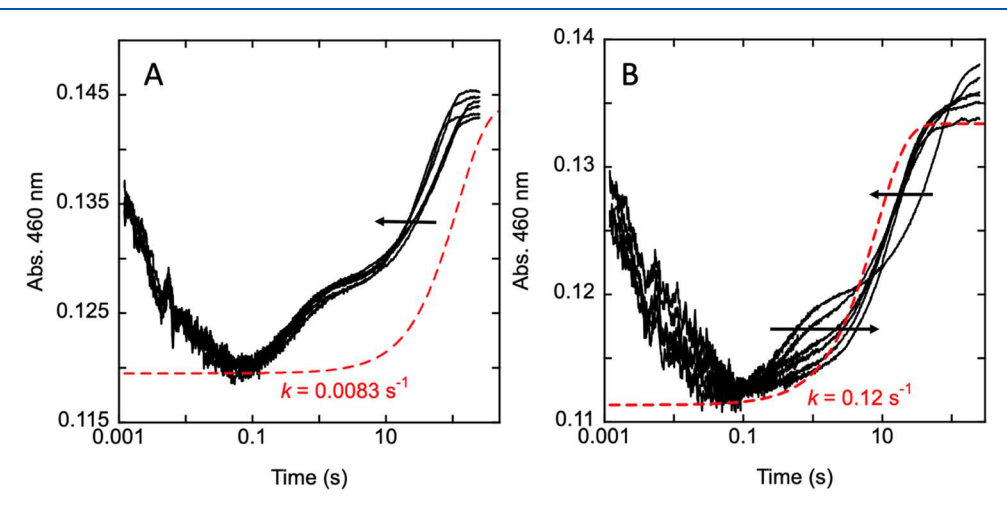


Figure 6. Effect of oxidant substrates on the reductive half-reaction of SmTGR. SmTGR (10.5  $\mu$ M) was mixed with NADPH (~8.9  $\mu$ M) and either oxidized glutathione (0, 5, 20, 40, 80, 160  $\mu$ M) (A) or oxidized SmTrx (0, 12, 21.5, 41.5, 76, 116  $\mu$ M) (B) under anaerobic conditions at 20 °C. The reaction was observed at 460 nm for two timeframes (0.0012–0.2 and 0.0012–200 s), and the 200 s traces shown were spliced together at 0.2 s to provide adequate time resolution for all phases. Arrows indicate increasing oxidant concentration. Exponential curves shown in red illustrate the limiting rate of turnover for each oxidant substrate relative to the data shown.

this ligand promoting deprotonation of Cys159. This is evident at both 450 and 540 nm. Interestingly, the 450 nm traces seemingly show that the extent of flavin reduction observed increases with added NADP<sup>+</sup>; however, this is likely a consequence of suppressed FAD-thiolate charge transfer transitions effectively revealing more of the FAD reduction at this wavelength.

Influence of Oxidant Substrates on the Reductive Half-Reaction. It is proposed that the C-terminal 596–597 cysteine pair acts as a tethered mobile electron carrier that in the disulfide state can accept two electrons from the 154, 159 cysteines and pass the electrons to Trx or to the 28–31 disulfide pair that is adjacent to a GSSG binding site (Figure 1). The data shown in Figures 2–5 suggest that the net passage of electrons out of the flavin is staged, coming to quasi-equilibrium states that have fractional distributions of electrons in multiple redox centers. In a bid to show at what stages of the reductive half-reaction electrons can leave TGR via reduction

of oxidant substrates, the reductive half-reaction was observed in the presence of SmTrx and GSSG (Figure 6).

These experiments included near-equimolar concentrations of SmTGR and NADPH as an attempt to limit inter-subunit redox chemistry. The assumption is that the phase of flavin reoxidation that has a half-life around 0.4 s corresponds to the accumulation of the reduced 596, 597 cysteine pair (Figure 3C). For reference, a curve defined by the observed rate of turnover under anaerobic conditions with GSSG is included in Figure 6A to illustrate the rate constant for the event limiting the rate of catalysis. The decay of this state is then rate-limiting conceivably because of the requirement for extensive reordering of the peptide to which this cysteine pair is tethered to both localize adjacent to and reduce the distant 28-31 disulfide. When SmTGR was mixed with NADPH and GSSG the rate of the last phase is largely unchanged with GSSG concentration and more rapid than the rate of turnover with this oxidant. Ignoring the complexities of potential

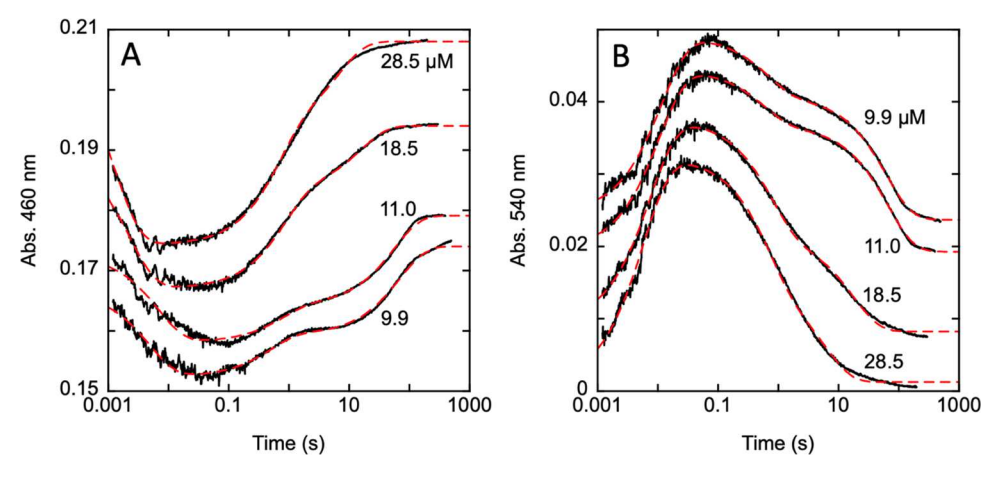


Figure 7. Effect of SmTGR concentration on the observed kinetics. SmTGR (9.9, 11.0, 18.5, 28.5  $\mu$ M) was mixed with NADPH (10  $\mu$ M) under anaerobic conditions at 20 °C. The reactions were observed at 460 nm (A) and 540 nm (B) for two timeframes (0.0012–0.2 and 0.0012–(200–500) s) and the traces were spliced together at 0.2 s to provide adequate time resolution for all phases. The traces were fit to a linear combination of three exponential terms according to eq 2. Traces were separated for clarity.

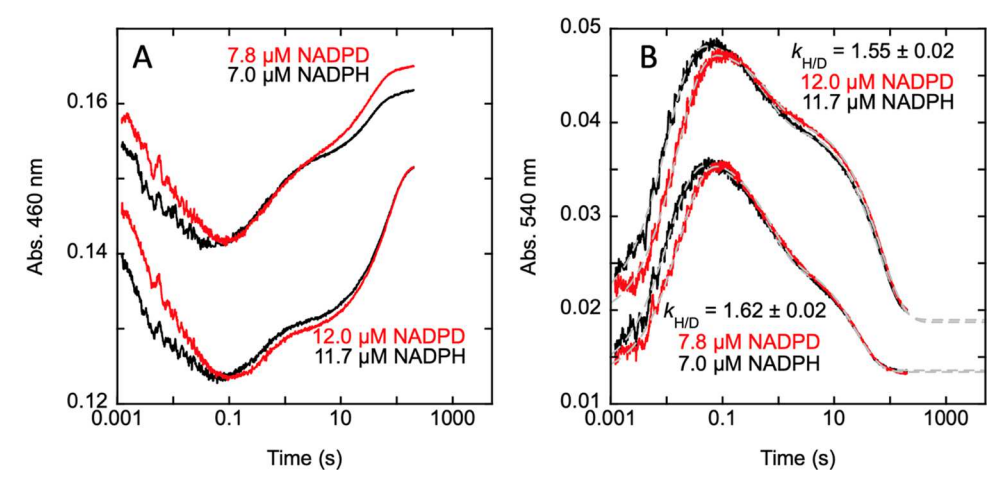


Figure 8. Effect of [4S- $^2$ H] NADPD on the reductive half-reaction of SmTGR. SmTGR (13.5  $\mu$ M) was mixed with NADPH (7.0, 11.7  $\mu$ M) or [4S- $^2$ H] NADPD (7.8, 12.0  $\mu$ M) under anaerobic conditions at 20 °C. The reaction was observed at 460 nm (A) and 540 nm (B) for two timeframes (0.0012–0.2 and 0.0012–200 s) and the 200 s traces shown were spliced together at 0.2 s to provide adequate time resolution for all phases. The traces were fit to a linear combination of three exponential terms.

interdimer redox chemistry, these data added to the data shown in Figures 2–5 suggest that electron transfer to the 28–31 disulfide is not rate-limiting in GSSG reduction.

SmTrx was also evaluated for the effect on the reductive half-reaction. The primary effect of this oxidant is diminishment of the stepped appearance for reoxidation of the flavin. According to the proposed model, this would suggest that electrons are less prone to accumulate on the \$96–597 cysteine pair and instead shuttle to the Trx disulfide at a rate that exceeds that for transmittance of electrons to the 28–31 cysteine pair or GSSG and this balance of rates is observed in the measured turnover numbers (Figure 2). Again, for reference, a curve defined by the observed rate of turnover under anaerobic conditions with SmTrx is included in Figure 6B to illustrate the rate constant for the event(s) limiting the rate of catalysis.

Effect of SmTGR Concentration on the Kinetics of the Reductive Half-Reaction. To assess the influence of interdimer electron transfer, varied SmTGR concentrations were observed in the reductive half-reaction with a fixed concentration of NADPH. These data show that increasing

concentrations of enzyme cause flavin reoxidation to transition from being biphasic and to largely monophasic (Figure 7A).

This change in shape is derived primarily from an increase in the amplitude of the first reoxidation phase such that it dominates the overall increase in absorption. This progression suggests that electrons that migrate to the 596-597 disulfide are readily transferred to nearby dimers and that this phenomenon is more prevalent with a high fraction of enzyme that is unreacted. These trends are mirrored at 540 nm where it is observed that decay of FAD-thiolate charge transfer also progressively loses the stepped character at higher SmTGR concentrations. The range of SmTGR concentrations used is too narrow to provide truly monophasic reoxidation at the highest SmTGR concentrations in that flavin reoxidation at both wavelengths retains evidence of biphasic character for all concentrations of SmTGR. Nonetheless, it is apparent that an excess of nonreacting SmTGR provides an alternate path for electrons to depart from the sequential chain of redox reactions required for normal catalysis. These data suggest that movements of the C-terminus are indiscriminate and likely complicate interpretation of SmTGR kinetic data.

Kinetic Isotope Effects on the Reductive Half-Reaction. As further evidence of the validity of the proposed mechanism, SmTGR was reacted separately with limiting NADPH and limiting [4S-<sup>2</sup>H] NADPD (Figure 8). Despite that flavin reduction and reoxidation occurs too rapidly to determine kinetic isotope effect (KIE) values for these events, if our mechanistic assignments are correct a KIE should be observed for the formation of the FAD-159 thiolate charge transfer absorption. This is expected if the hydride transferred to the NS of the flavin is then delivered to the 159 sulfur of the 154–159 cysteine and is then lost to form the charge transfer feature (Figure 1).

As indicated in Figure 3A, it is not possible to saturate with NADPH to observe this effect, as only NADPH concentrations equal to or less than the enzyme concentration resolve phases associated with electron redistribution within the enzyme. As such, NADPH and [4S-2H] NADPD were reacted with SmTGR at two concentrations and the data were compared. In Figure 8, we observed that a KIE can readily be discerned for the formation of what was assigned as the FAD-159 thiolate charge transfer at 540 nm. When these data were fit to a linear combination of three exponentials according to eq 2, the measured isotope effects for the two concentrations were 1.55 and 1.62, suggesting that these report a value that is independent of NADPH binding processes. The low normal effect is consistent with a nonlinear transition state for loss of the proton to form the 159 thiolate. The only residue within a 4 Å radius of Cys159 that is also capable of accepting a proton is His571. Presumably the modest KIE value reflects the positioning of these two residues once the 154-159 disulfide has been reduced. This establishes that the hydride transferred from NADPH to the FAD N5 is then passed as a hydride to the 159 residue of the 154-159 cysteine and then matures to form the thiolate before electrons are passed to subsequent disulfides within the protein and/or to those on other SmTGR subunits.

#### CONCLUSIVE REMARKS

The unusual approach exhibited by Schistosoma to limit oxidative damage has resulted in heavy reliance on a single enzyme to survive inside the host. Efforts to inhibit helminthic TGRs have identified numerous molecules that slow or halt activity.<sup>33–38</sup> The mode of inhibition for some of these molecules has been established by X-ray crystal structures, 33,34 while the mode of action for others either is proposed by docking or remain unknown.<sup>35</sup> Despite its established importance, Schistosoma TGR has hitherto had no comprehensive transient-state analysis reported. In a bid to baseline the kinetic behavior of TGR enzymes as a prelude to understanding the mode of action of known inhibitors, we have utilized the spectrophotometric reporting facility of the active site flavin cofactor. The FAD of SmTGR Sec597Cys reports reductive and oxidative steps that distribute electrons to the three disulfide pairs required to reduce GSSG and SmTrx. The data show that SmTGR binds and then accepts a hydride from NADPH very rapidly and then passes these electrons at near the same rate to the disulfide directly adjacent to the reduced flavin and back to NADP<sup>+</sup>. The loss of a proton from the most proximal cysteine (159) occurs with egress of NADP+ and yields intense FAD-thiolate charge transfer transitions. These electrons then migrate to a dynamic disulfide that exists on a disordered loop at the C-terminal end of the protein. The dynamic nature of this loop allows it

both to reduce SmTrx and reduce the final disulfide that, based on the structure, resides on the adjacent subunit. This third cysteine pair then can reduce GSSG that has been shown to bind proximally.<sup>11</sup> We propose that the lack of defined structure for the loop that carries the second disulfide creates a kinetic barrier for the reduction of GSSG and promotes interdimer electron transfer inducing SmTGR concentrationdependent changes to the observed kinetics. That the flavin can report each of these events, dictates that electrons move freely in the forward and reverse directions such that the net extent of oxidation of the flavin changes with the distribution of electrons. Scheme 1 summarizes the proposed binding and catalytic redox chemistry of SmTGR based on the data presented. The central horizontal column shown in gray summarizes the reductive half-reaction. Rate constants indicated in blue are observed rate constants for approaches to semi-equilibrium states and do not represent intrinsic rates for any step in the reaction. SmTrx and GSSG are shown to undergo reduction by interacting with the 595, 597, and 28, 31 cysteine pairs, respectively, and their overall rate of reduction is described by the limiting rate of turnover without assignment to a specific step (blue arrows). The scheme does not show pathways for inter-subunit electron transfer.

# ASSOCIATED CONTENT

## **Accession Codes**

S. mansoni thioredoxin/glutathione reductase (SmTGR)—A0A3Q0KFL1. S. mansoni thioredoxin (SmTrx)—Q8T9N5. S. cerevisiae hexokinase—P04807. L. mesenteroides glucose-6-phosphate dehydrogenase—C2KM82.

## AUTHOR INFORMATION

## **Corresponding Author**

Graham R. Moran – Department of Chemistry and Biochemistry, Loyola University Chicago, Chicago, Illinois 60660, United States; orcid.org/0000-0002-6807-1302; Phone: (773)508-3756; Email: gmoran3@luc.edu

#### Authors

Madison M. Smith – Department of Chemistry and Biochemistry, Loyola University Chicago, Chicago, Illinois 60660, United States

**Tyler B. Alt** – Department of Chemistry and Biochemistry, Loyola University Chicago, Chicago, Illinois 60660, United

David L. Williams — Department of Microbial Pathogens and Immunity, Rush University Medical Center, Chicago, Illinois 60612, United States

Complete contact information is available at: https://pubs.acs.org/10.1021/acs.biochem.3c00051

## **Author Contributions**

§M.M.S. and T.B.A. contributed equally to the production of this article.

## Notes

The authors declare no competing financial interest.

#### ACKNOWLEDGMENTS

This research was supported by National Science Foundation Grants CHE 1904480 and CHE 2203593 to G.R.M. and by a National Institutes of Health Grant NIAID R33AI127635 to D.L.W.

#### REFERENCES

- (1) Colley, D. G.; Bustinduy, A. L.; Secor, W. E.; King, C. H. Human schistosomiasis. *Lancet* **2014**, 383, 2253–2264.
- (2) Skelly, P. Fighting killer worms. Sci. Am. 2008, 298, 94-99.
- (3) Doenhoff, M. J.; Cioli, D.; Utzinger, J. Praziquantel: mechanisms of action, resistance and new derivatives for schistosomiasis. *Curr. Opin. Infect. Dis.* **2008**, *21*, 659–667.
- (4) Wang, W.; Wang, L.; Liang, Y. S. Susceptibility or resistance of praziquantel in human schistosomiasis: a review. *Parasitol Res* **2012**, *111*, 1871–1877.
- (5) Utzinger, J.; Raso, G.; Brooker, S.; De Savigny, D.; Tanner, M.; Ornbjerg, N.; Singer, B. H.; N'Goran, E. K. Schistosomiasis and neglected tropical diseases: towards integrated and sustainable control and a word of caution. *Parasitology* **2009**, *136*, 1859–1874.
- (6) Colley, D. G.; Secor, W. E. Immunology of human schistosomiasis. *Parasite Immunol.* **2014**, *36*, 347–357.
- (7) Kuntz, A. N.; Davioud-Charvet, E.; Sayed, A. A.; Califf, L. L.; Dessolin, J.; Arner, E. S.; Williams, D. L. Thioredoxin glutathione reductase from *Schistosoma mansoni*: an essential parasite enzyme and a key drug target. *PLoS Med.* **2007**, *4*, No. e206.
- (8) Tripathi, T.; Suttiprapa, S.; Sripa, B. Unusual thiol-based redox metabolism of parasitic flukes. *Parasitol. Int.* **2017**, *66*, 390–395.
- (9) Williams, D. L.; Bonilla, M.; Gladyshev, V. N.; Salinas, G. Thioredoxin glutathione reductase-dependent redox networks in platyhelminth parasites. *Antioxid. Redox Signaling* **2013**, *19*, 735–745.
- (10) Alger, H. M.; Williams, D. L. The disulfide redox system of *Schistosoma mansoni* and the importance of a multifunctional enzyme, thioredoxin glutathione reductase. *Mol. Biochem. Parasitol.* **2002**, *121*, 129–139.
- (11) Angelucci, F.; Dimastrogiovanni, D.; Boumis, G.; Brunori, M.; Miele, A. E.; Saccoccia, F.; Bellelli, A. Mapping the catalytic cycle of *Schistosoma mansoni* thioredoxin glutathione reductase by X-ray crystallography. *J. Biol. Chem.* **2010**, 285, 32557–32567.
- (12) Schulz, G. E.; Karplus, P. A. High resolution structure and catalytic action of human glutathione reductase. *Biochem. Soc. Trans.* 1988, 16, 81–84.
- (13) Fritz-Wolf, K.; Jortzik, E.; Stumpf, M.; Preuss, J.; Iozef, R.; Rahlfs, S.; Becker, K. Crystal structure of the *Plasmodium falciparum* thioredoxin reductase-thioredoxin complex. *J. Mol. Biol.* **2013**, 425, 3446–3460.
- (14) Huang, H. H.; Day, L.; Cass, C. L.; Ballou, D. P.; Williams, C. H., Jr.; Williams, D. L. Investigations of the catalytic mechanism of thioredoxin glutathione reductase from *Schistosoma mansoni*. *Biochemistry* **2011**, *50*, 5870–5882.
- (15) Rendón, J. L.; Miranda-Leyva, M.; Guevara-Flores, A.; Martinez-Gonzalez, J. J.; Del Arenal, I. P.; Flores-Herrera, O.; Pardo, J. P. Insight into the Mechanistic Basis of the Hysteretic-Like Kinetic Behavior of Thioredoxin-Glutathione Reductase (TGR). *Enzyme Res.* **2018**, 2018, No. 3215462.
- (16) Plancarte, A.; Nava, G. Purification and kinetic analysis of cytosolic and mitochondrial thioredoxin glutathione reductase extracted from *Taenia solium cysticerci*. Exp. Parasitol. **2015**, 149, 65–73
- (17) Kalita, P.; Shukla, H.; Shukla, R.; Tripathi, T. Biochemical and thermodynamic comparison of the selenocysteine containing and non-containing thioredoxin glutathione reductase of Fasciola gigantica. *Biochim. Biophys. Acta, Gen. Subj.* 2018, 1862, 1306–1316.
- (18) Moran, G. R.Anaerobic methods for the transient-state study of flavoproteins: The use of specialized glassware to define the concentration of dioxygen. In *Methods in Enzymology*; Elsevier B.V., 2019; Vol. 620, pp 27–49.
- (19) Timson, D. J.Praziquantel: An Enigmatic, Yet Effective, Drug. In *Schistosoma mansoni*; Timson, D. J., Ed.; Humana: New York, 2020; Vol. 2151, pp 1–8.
- (20) Li, F.; Lutz, P. B.; Pepelyayeva, Y.; Arner, E. S.; Bayse, C. A.; Rozovsky, S. Redox active motifs in selenoproteins. *Proc. Natl. Acad. Sci. U.S.A.* **2014**, *111*, 6976–6981.
- (21) Cheng, Q.; Arner, E. S. Selenocysteine Insertion at a Predefined UAG Codon in a Release Factor 1 (RF1)-depleted Escherichia coli

- Host Strain Bypasses Species Barriers in Recombinant Selenoprotein Translation. *J. Biol. Chem.* **2017**, 292, 5476–5487.
- (22) Reich, H. J.; Hondal, R. J. Why Nature Chose Selenium. ACS Chem. Biol. 2016, 11, 821-841.
- (23) Ste Marie, E. J.; Wehrle, R. J.; Haupt, D. J.; Wood, N. B.; van der Vliet, A.; Previs, M. J.; Masterson, D. S.; Hondal, R. J. Can Selenoenzymes Resist Electrophilic Modification? Evidence from Thioredoxin Reductase and a Mutant Containing alpha-Methylselenocysteine. *Biochemistry* **2020**, *59*, 3300–3315.
- (24) Maroney, M. J.; Hondal, R. J. Selenium versus sulfur: Reversibility of chemical reactions and resistance to permanent oxidation in proteins and nucleic acids. *Free Radical Biol. Med.* **2018**, 127, 228–237.
- (25) Nauser, T.; Steinmann, D.; Grassi, G.; Koppenol, W. H. Why selenocysteine replaces cysteine in thioredoxin reductase: a radical hypothesis. *Biochemistry* **2014**, *53*, 5017–5022.
- (26) Massey, V.; Williams, C. H., Jr. On the reaction mechanism of yeast glutathione reductase. *J. Biol. Chem.* **1965**, *240*, 4470–4480.
- (27) Böhme, C. C.; Arscott, L. D.; Becker, K.; Schirmer, R. H.; Williams, C. H., Jr. Kinetic characterization of glutathione reductase from the malarial parasite *Plasmodium falciparum*. Comparison with the human enzyme. *J. Biol. Chem.* **2000**, 275, 37317–37323.
- (28) Zanetti, G.; Williams, C. H., Jr. Characterization of the active center of thioredoxin reductase. J. Biol. Chem. 1967, 242, 5232–5236.
- (29) Huber, P. W.; Brandt, K. G. Kinetic studies of the mechanism of pyridine nucleotide dependent reduction of yeast glutathione reductase. *Biochemistry* **1980**, *19*, 4568–4575.
- (30) Williams, C. H.; Arscott, L. D.; Muller, S.; Lennon, B. W.; Ludwig, M. L.; Wang, P. F.; Veine, D. M.; Becker, K.; Schirmer, R. H. Thioredoxin reductase two modes of catalysis have evolved. *Eur. J. Biochem.* **2000**, *267*, 6110–6117.
- (31) Crozier-Reabe, K.; Moran, G. R. Form follows function: structural and catalytic variation in the class a flavoprotein monoxygenases. *Int. J. Mol. Sci.* **2012**, *13*, 15601–15639.
- (32) Rietveld, P.; Arscott, L. D.; Berry, A.; Scrutton, N. S.; Deonarain, M. P.; Perham, R. N.; Williams, C. H., Jr. Reductive and oxidative half-reactions of glutathione reductase from *Escherichia coli*. *Biochemistry* **1994**, *33*, 13888–13895.
- (33) Silvestri, I.; Lyu, H.; Fata, F.; Boumis, G.; Miele, A. E.; Ardini, M.; Ippoliti, R.; Bellelli, A.; Jadhav, A.; Lea, W. A.; Simeonov, A.; Cheng, Q.; Arner, E. S. J.; Thatcher, G. R. J.; Petukhov, P. A.; Williams, D. L.; Angelucci, F. Fragment-Based Discovery of a Regulatory Site in Thioredoxin Glutathione Reductase Acting as "Doorstop" for NADPH Entry. ACS Chem. Biol. 2018, 13, 2190—2202.
- (34) Fata, F.; Silvestri, I.; Ardini, M.; Ippoliti, R.; Di Leandro, L.; Demitri, N.; Polentarutti, M.; Di Matteo, A.; Lyu, H.; Thatcher, G. R. J.; Petukhov, P. A.; Williams, D. L.; Angelucci, F. Probing the Surface of a Parasite Drug Target Thioredoxin Glutathione Reductase Using Small Molecule Fragments. *ACS Infect. Dis.* **2021**, *7*, 1932–1944.
- (35) Li, G.; Guo, Q.; Feng, C.; Chen, H.; Zhao, W.; Li, S.; Hong, Y.; Sun, D. Synthesis of oxadiazole-2-oxide derivatives as potential drug candidates for schistosomiasis targeting SjTGR. *Parasites Vectors* **2021**, *14*, No. 225.
- (36) Tripathi, T.; Chetri, P. B. Potent Inhibitors of Thioredoxin Glutathione Reductase: Grail of Anti-Schistosome Drug within Reach? *ACS Infect. Dis.* **2020**, *6*, 893–895.
- (37) Eweas, A. F.; Allam, G. Targeting thioredoxin glutathione reductase as a potential antischistosomal drug target. *Mol. Biochem. Parasitol.* **2018**, 225, 94–102.
- (38) Sayed, A. A.; Simeonov, A.; Thomas, C. J.; Inglese, J.; Austin, C. P.; Williams, D. L. Identification of oxadiazoles as new drug leads for the control of schistosomiasis. *Nat. Med.* **2008**, *14*, 407–412.